J Solid State Electrochem (2012) 16:3581–3586
DOI 10.1007/s10008-012-1790-8

ORIGINAL PAPER

Synthesis of nano-$LiFePO_4$ particles with excellent electrochemical performance by electrospinning-assisted method

Mingjuan Li · Liqun Sun · Kai Sun · Shihua Yu · Rongshun Wang · Haiming Xie

Received: 6 April 2012 / Revised: 26 May 2012 / Accepted: 29 May 2012 / Published online: 9 June 2012

Abstract Nanoscale $LiFePO_4$/C particles are synthesized using a combination of electrospinning and annealing. The important advantages of electrospinning technique are the production of separated nanofiber precursor, enabling the precursor particles arrangement to be changed, impeding the growth and agglomeration of the $LiFePO_4$ particles during the heat treatment, and contributing to the formation of nanosized $LiFePO_4$ particles. In this study, polyvinylpyrrolidone (PVP) is used as the fiber-forming agent in the electrospinning method, and also provides a reducing agent and carbon source. In situ carbon-coated $LiFePO_4$ particles are obtained by the pyrolysis of PVP during the thermal treatment. The $LiFePO_4$ particles are coated with and connected by interlaced carbons, and are uniformly distributed in the size range 50–80 nm. It is found that the as-prepared nanoscale $LiFePO_4$/C composite has a desirable electrochemical performance. It has discharge capacities of 163.5 mA h g^{-1} and 110.7 mA h g^{-1} at rates of 0.1 C and 10 C, respectively. In addition, this cathode has excellent cyclability with a capacity loss of less than 3 % at 0.1 C and 5 % at 5 C after 500 cycles. An effective synthesis and processing method is presented for obtaining nanosized $LiFePO_4$ with high electrochemical performance.

M. Li · L. Sun · K. Sun · S. Yu · R. Wang (✉) · H. Xie (✉)
Department of Chemistry, Institute of Functional Materials,
Northeast Normal University,
Changchun, Jilin 130024, People's Republic of China
e-mail: wangrs@nenu.edu.cn
e-mail: xiehm136@nenu.edu.cn

M. Li · L. Sun · K. Sun · S. Yu · R. Wang · H. Xie
LIB Engineering Laboratory,
Materials Science and Technology Center,
Changchun, Jilin 130024, People's Republic of China

Keywords Lithium-ion battery · Cathode · Nanosized $LiFePO_4$ · Electrospinning

Introduction

In the near future, there will be a huge market for rechargeable Li-ion batteries for use in electric vehicles and energy-storage systems. Among the various candidates for suitable cathode materials in Li-ion batteries, olivine-type $LiFePO_4$ has attracted significant interest because of its advantages of high thermal stability and long cycle life. However, it has an inherently poor electronic conductivity (~10^{-9} S cm^{-1}) and slow Li-ion diffusivity, which are disadvantages in its application in secondary batteries [1,2].

Considerable efforts have been made to overcome electronic and ionic transport limitations using cationic doping [3–5], carbon coating [6–8], and the synthesis of smaller particles [9–11]. In recent years, nanostructured materials have attracted great interest in the field of Li-ion batteries, mainly because of their substantial advantages in terms of mass transport. Compared with other systems, transport in nanoparticle systems typically involves shorter transport lengths for both electronic and Li^+ transport, higher electrode–electrolyte contact areas, and better accommodation of the strain of Li^+ insertion/extraction. Decreasing the particle size in the active materials increases the rate of diffusion of Li ions in $LiFePO_4$ and improves the rate capability of the sample.

To obtain nanoscale $LiFePO_4$ particles, numerous synthetic strategies have been developed, such as sol–gel [12], hydrothermal [13], co-precipitation [14], template-mediated [15], ball-milling followed by solid-state reactions [16], and microwave solvothermal methods [17].

The use of electrospinning as a method for producing nanostructures of advanced materials such as polymers, metal oxides, and metals is currently attracting much research interest [18–21]. Briefly, electrospinning is a technique for producing fibers of micrometer and nanometer diameters by creating a continuous filament by exposing a polymer solution or polymer melt to very high electric fields [22]. Hosono et al. synthesized triaxial $LiFePO_4$ nanowires with a vapor-grown carbon-fiber (VGCF) core-column and a carbon shell using the electrospinning method [23]. The thickness of the $LiFePO_4$ nanowires (about 500 nm up to 1 mm in diameter) constrains their performance. Zhu et al. have synthesized carbon-coated $LiFePO_4$ nanowires of diameter around 100 nm using electrospinning [24], and these show an improved electrochemical performance. However, the performance is still not high enough to be satisfactory.

In this study, we synthesized in situ carbon-coated $LiFePO_4$ nanoparticles of size 50–80 nm via an electrospinning-assisted method. Polyvinylpyrrolidone (PVP) was used as the polymer matrix. Its excellent fiber-forming ability and chemical stability facilitate the formation of nanofiber precursors. Furthermore, the residual carbon pyrolyzed from PVP plays the role of a conductive additive to improve the electronic conductivity of the product. As-prepared $LiFePO_4$/C exhibits a high discharge capacity and good rate performance. The advantages of using an electrospinning method for the synthesis of $LiFePO_4$ with respect to the morphology, size, and electrochemical performance of the $LiFePO_4$ in comparison with that obtained using a normal ball-milling method without electrospinning are discussed.

Experimental

Synthesis

Nanofiber precursor preparation: the nanofibers were fabricated by electrospinning a homogeneous dispersed solution of PVP (Aldrich, M_w=20,000), lithium hydroxide, and hydrated iron phosphate. The materials used were of analytical grade and they did not need to be dried prior to use.

In a typical procedure, different weights of PVP (0.6, 1.0, and 1.8 g) were mixed with ethanol (15 mL) in a small conical flask, followed by magnetic stirring for 1 h to ensure the dissolution of PVP. At the same time, 1.10 g of $LiOH{\cdot}H_2O$ and 4.67 g of $FePO_4{\cdot}2H_2O$ were dispersed in distilled water and added to the polymer solution, with intensive stirring, to obtain a homogeneous system. The spinning solutions contained different weight concentrations (i.e., 3 %, 5 %, and 8 % relative to the weight of the solution) of PVP in the mixture solutions. The resultant precursor was poured into a syringe connected to a plastic needle, and a Cu wire attached to a high-voltage generator was placed in the solution. A direct-current electric field of 15 kV was applied between the needle and the Al foil target used for collection; the flow rate was approximately 0.8 mL h^{-1}. The electrospun fibers were calcined at 350 °C for 2 h and 650 °C for 8 h under a N_2 atmosphere. The as-prepared $LiFePO_4$/C is denoted by LFP1/C. For comparison, a mixture of $LiOH{\cdot}H_2O$/PVP/$FePO_4{\cdot}2H_2O$ was ball-milled for 10 h, dried directly in an oven, and calcined under the same conditions as described above to synthesize $LiFePO_4$, denoted by LFP2/C.

Characterization and electrochemical measurements

Scanning electron microscopy (SEM; Hitachi S-3500V) was used to examine the surface morphologies of the samples. The internal morphologies were studied using high-resolution transmission electron microscopy (HR-TEM; JEOL TEM-2000FXII). The crystal structure of $LiFePO_4$/C was investigated by X-ray diffraction (XRD) analysis with a Rigaku P/max 2200VPC using Cu Kα radiation (λ= 1.5406 Å). Raman measurements were performed on a Jobin Yvon HR-800 microscopic confocal Raman spectrometer with 428-nm excitation from an Ar^+ laser source.

The electrochemical characterization was performed using 2025 coin-type cells assembled in an Ar-filled glove box. The cathodes were fabricated by mixing 85 wt.% $LiFePO_4$/C with 10 wt.% acetylene black and 5 wt.% poly (vinylidene fluoride) in *N*-methylpyrrolidone. Electrodes with active material loadings of about 2 mg cm^{-2} were prepared using Al foil as the current collector. The test cell consisted of the cathode and Li-foil anode separated by a porous Celgard 2400 film, and 1 M $LiPF_6$ in ethylene carbonate (EC) and diethyl carbonate (DEC) (1:1 v/v) as the electrolyte. The cells were tested at room temperature over the voltage range 2.5–4.2 V.

Results and discussion

Morphology of the $LiFePO_4$/C precursor

The SEM image of the $FePO_4{\cdot}2H_2O$ raw material in Fig. 1a shows an array of uniform bundles of nanorods with a primary particle size of about 60 nm, which is the premise that $FePO_4{\cdot}2H_2O$ particles can be electrospun into nanofibers. Figure 1b–d shows the morphologies of the as-electrospun nanofibers produced from the spinning solutions containing different weight concentrations of PVP. At a low PVP concentration (3 %), the sample shows a bead morphology and few nanofibers (Fig. 1b), as a result of the low viscosity of the spinning solution. Nanofibers with an average diameter of 170±20 nm are formed when the concentration of PVP in the spinning solution is 5 % (Fig. 1c). It can be seen that uniform nanofibers are randomly oriented

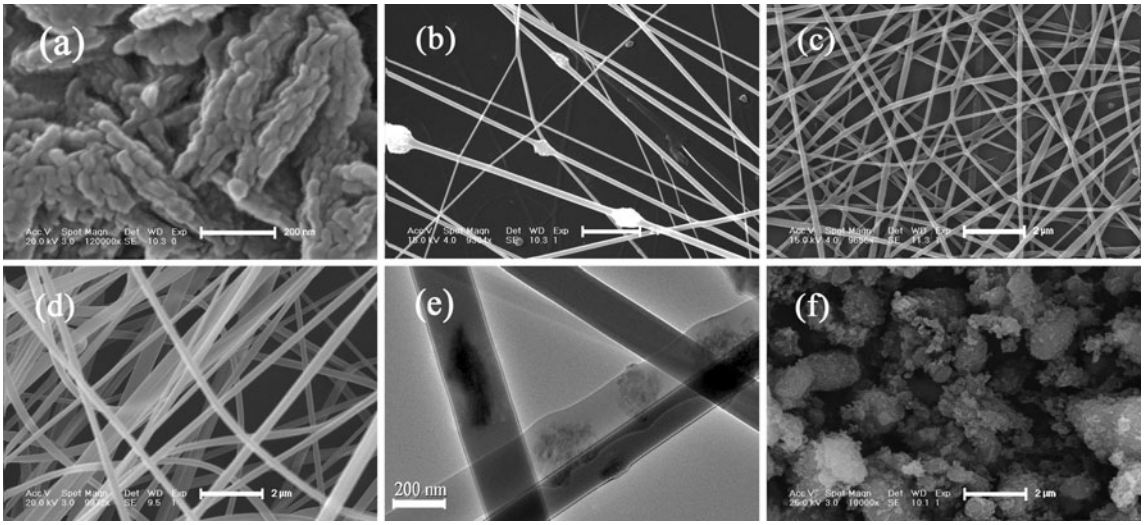

Fig. 1 **a** SEM image of $FePO_4 \cdot 2H_2O$ raw material; **b**–**d** SEM images of as-electrospun nanofibers with PVP weight concentrations of 3 %, 5 %, and 8 %; **e** TEM image of the nanofiber precursor with 5 % PVP; and **f** SEM image of the precursor obtained using ball-milling method

on the substrate and are interwoven as a spider's web. Further addition of PVP induces an increase in the viscosity of the spinning solution, and non-uniform nanofibers with larger diameters, ranging from 300 to 500 nm (Fig. 1d), are obtained when the PVP concentration is increased to 8 %. This increase in diameter with viscosity has been previously reported for many electrospun polymer fibers [25]. Therefore, 5 % PVP was chosen as the optimum weight concentration in this work. The TEM image of nanofibers produced from the electrospinning solution with 5 % PVP is shown in Fig. 1e. The precursor fibers show some rough spots on the surface where the precursor particles are located, indicating that the precursor particles are distributed both inside and on the surface of the precursor fibers. The SEM image of the precursor obtained from normal ball-milling is shown in Fig. 1f. It can be seen that the main difference between the two samples is that the latter precursor consists of small clusters and agglomerates; this is bound to be inferior to separated nanofibers, which suppress agglomeration of the subsequent product, $LiFePO_4$.

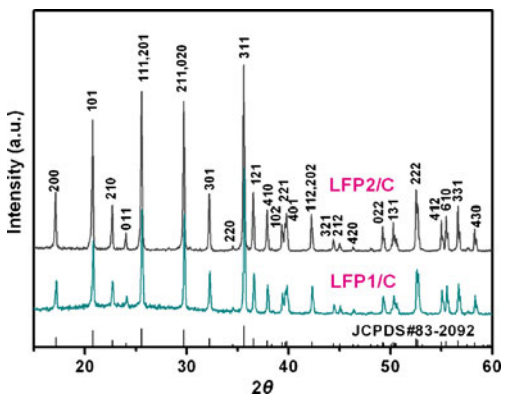

Fig. 2 XRD patterns of LFP1/C and LFP2/C composites

Structural characterization and morphology studies of $LiFePO_4$/C composites

$LiFePO_4$/C nanoparticles were obtained after heat treatment of the above as-electrospun nanofibers and of the precursor obtained by normal ball-milling. The PVP is decomposed into carbon at high temperature, and is used as a reducing agent and conductive carbon source.

Figure 2 shows the XRD patterns of LFP1/C and LFP2/C. They exhibit similar patterns, which can be attributed to an ordered $LiFePO_4$ olivine structure indexed to orthorhombic Pnmb (JCPDS card no. 83-2092). However, the lattice constant of LFP1/C is smaller than that of LFP2/C, as shown in Table 1. It is well known that Li-ion diffusion in the lattice is uniaxial along the *b*-direction. The smaller *b* value of LFP1/C enhances the Li-ion diffusion rate. In addition, it can be clearly seen that the peak intensity of LFP2/C is stronger than that of LFP1/C, indicating an increase in crystallinity, which can occur as a result of grain-size growth, ordering of local structures, and release of lattice strain [26].

Figure 3 shows the morphologies of the $LiFePO_4$/C products. It can be seen from Fig. 3a that the LFP1 grains are arranged along the direction of the nanofiber precursor and show a rope-knot shape, which may be related to the choice of solid–liquid system and the high-temperature treatment. After the heat treatment, PVP nanofibers can

Table 1 Structure lattice parameters and cell volumes of LFP1/C and LFP2/C composites

Sample	*a* (Å)	*b* (Å)	*c* (Å)	*V* (Å^3)
LFP1/C	10.313	5.999	4.692	290.28
LFP2/C	10.332	6.009	4.694	291.43

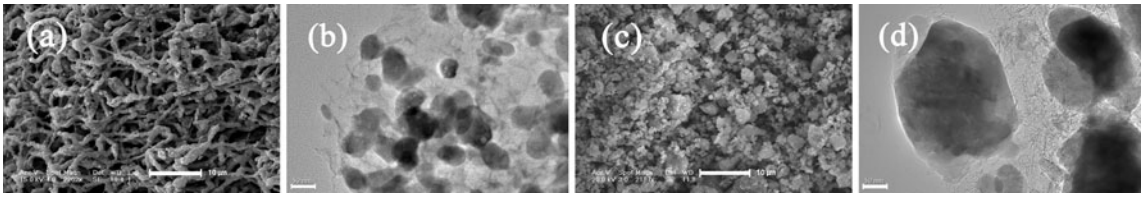

Fig. 3 **a**, **b** SEM and TEM images of LFP1/C obtained by electrospinning; **c**, **d** SEM and TEM images of LFP2/C produced without electrospinning

effectively transform into carbon network. The LFP1/C particles are coated with the interlaced carbon and have a uniform morphology with a narrow size distribution in the range 50–80 nm, as shown in Fig. 3b. The carbon networks among the particles inhibit the agglomeration of $LiFePO_4$ particles and improve the electronic conductivity of the material. The SEM and TEM images of LFP2/C, which did not undergo electrospinning treatment, display marked differences in its particle size and morphology. Figure 3c shows that LFP2/C consists of irregularly shaped particles and agglomeration is extensive. The single-particle size of LFP2/C (up to 200 nm) is much larger than that of LFP1/C, as shown in Fig. 3d; this is consistent with the XRD analysis. These results indicate that electrospinning achieves a homogeneous distribution of raw materials and changes the precursor particles arrangement, which inhibits the growth of $LiFePO_4$ particles.

On the basis of the TEM investigation, we performed Raman measurements to further investigate the structure of the carbon coating. Figure 4 shows the Raman spectra of pure $LiFePO_4$ and LFP1/C. The sharp band at 950 cm^{-1} and the two weak bands at 995 and 1,068 cm^{-1} in Fig. 4a can be attributed to the symmetric PO_4^{3-} stretching vibration of $LiFePO_4$ [27]. There is no band attributable to the presence of PVP, indicating that there is no carbon coating. In contrast, the broad bands in Fig. 4b, which are characteristic of carbon, along with the weak PO_4^{3-} bands, suggest a coating of structurally ordered carbon on $LiFePO_4$. The peak at 950 cm^{-1} observed for pure $LiFePO_4$ becomes weaker in the LFP/C composite spectra as a result of the presence of carbon peaks, which may overlap with it. The strong bands at around 1,358 and 1,606 cm^{-1} can be attributed to the D-band (sp^3 disorder-induced phonon mode) and G-band (sp^2 graphite band) of carbon, respectively [28]. The intensity ratio of the D-band to the G-band is estimated to be about 0.79. The I_D/I_G value generally provides a useful index for comparing the degree of crystallinity of various carbon materials. It has been reported that a decreasing D/G intensity means a decreasing sp^3/sp^2 ratio and increasing electronic conductivity of the material [29]. The low D/G ratio therefore implies a highly ordered carbon structure, contributing to the enhancement of the electronic conductivity and electrochemical performance of $LiFePO_4$/C. At room temperature, the electronic conductivity of LFP1/C is 9.8×10^{-2} S cm^{-1}, which is nearly eight orders of magnitude greater than that of pure $LiFePO_4$ (10^{-9} S cm^{-1}) [5]. Therefore, PVP in the system can therefore be considered not only as a fiber-shaping agent to tailor the morphology, but also as a carbon source.

Electrochemical performances of LFP1/C and LFP2/C

To ascertain the influence of the $LiFePO_4$ particle size on the electrochemical performance, the electrochemical behaviors

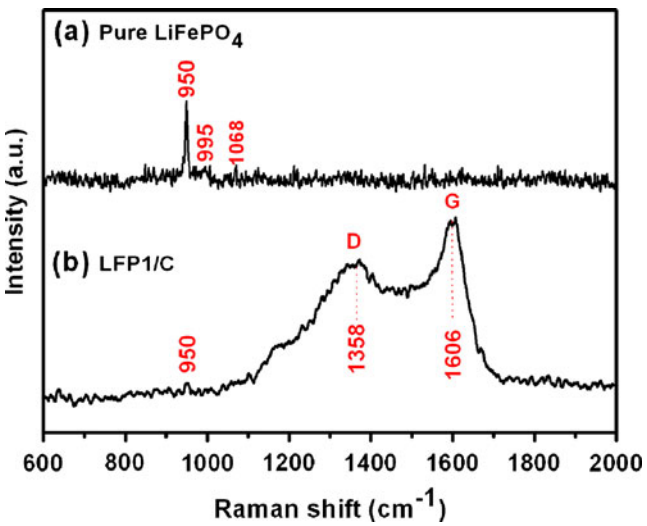

Fig. 4 Raman spectra of pure $LiFePO_4$ and LFP1/C composites

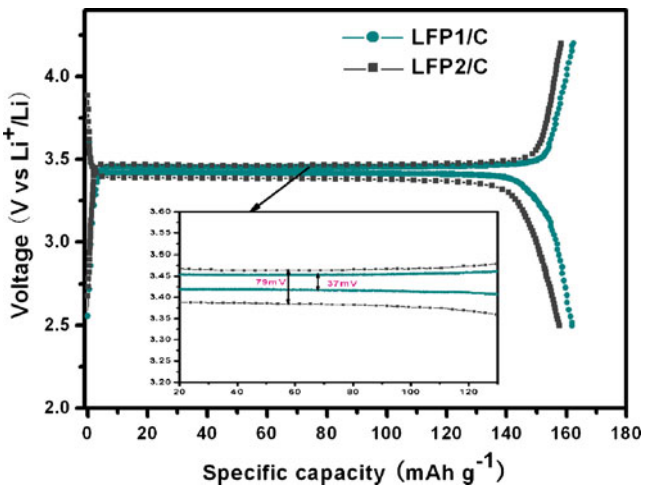

Fig. 5 Initial charge/discharge profiles of LFP1/C and LFP2/C cathodes at a rate of 0.2 C rate; the *inset* shows a magnification of the flat region

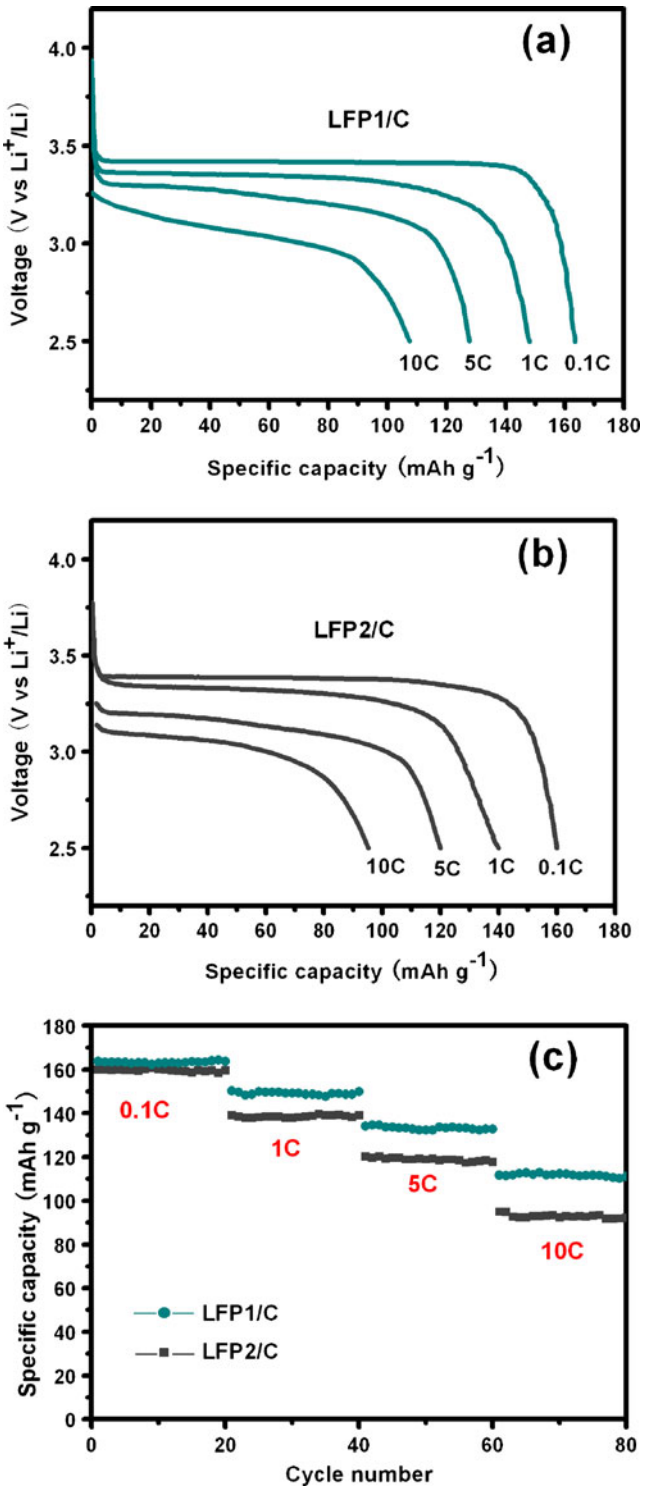

Fig. 6 Rate performance of $LiFePO_4$/C composite (0.1–10 C): **a** discharge curve of LFP1/C at different discharge rates, **b** discharge curve of LFP2/C at different discharge rates, and **c** comparison of rate capabilities of LFP1/C and LFP2/C

of the prepared materials were studied using galvanostatic tests. Figure 5 compares the initial charge/discharge profiles of the LFP1/C and LFP2/C cathodes. They exhibit a flat and long voltage plateau at ~3.4 V and display a very small

Table 2 Comparison of rate performances at room temperature for selected $LiFePO_4$ nanowires and those of our samples

Samples	Discharge capacity (mAh g^{-1})			
	0.1 C	1 C	5 C	10 C
LFP1/C	163.5	148	132	110.7
LFP2/C	160	139	120	95
$LiFePO_4$ nanowires (reference [25])	169	150	114	93
SCNW-LFP nanowires (reference [26])	160 (0.06 C)	130 (0.6 C)	80 (6 C)	–

charge/discharge polarization at a rate of 0.2 C. As shown in the plot, the charging/discharging potentials are around 3.453 V/3.416 V for LFP1/C and 3.463 V/3.384 V for LFP2/C. The small polarization of 37 mV for LFP1/C in comparison with that of 79 mV for LFP2/C reflects the good kinetics of LFP1/C, especially considering the low electrochemical diffusion rate of Li ions in a solid phase. The initial discharge capacities for LFP1/C and LFP2/C are 161.9 mA h g^{-1} and 157.7 mA h g^{-1}, respectively, and the former capacity corresponds to 95 % of the theoretical capacity. This can be attributed to the fast redox reactions of the LFP1/C nanoparticles, which provide an increased contact area between the active material and the electrolyte, and shorter Li-ion diffusion pathways.

Figure 6 shows the rate performances of as-prepared LFP1/C and LFP2/C. Four different rates (0.1 C, 1 C, 5 C, and 10 C) were selected to illustrate the cell behavior at intermediate rates. The LFP1/C composite shows a discharge capacity of 163.5 mA h g^{-1} at a low rate of 0.1 C, which is close to the theoretical capacity of 170 mA h g^{-1}. At higher rates, the LFP1/C composite exhibits an excellent rate capability with discharge capacities of 148, 132, and 110.7 mA h g^{-1} at rates

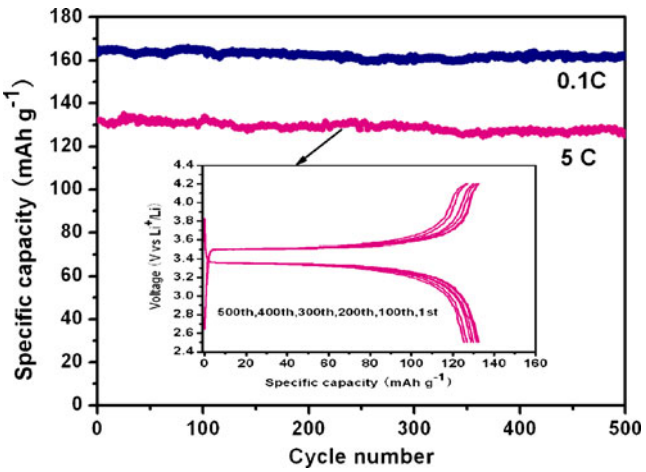

Fig. 7 Cycling performance of LFP1/C cathode at rates of 0.1 C and 5 C. The *inset* shows the charge/discharge curves at a rate of 5 C

of 1, 5, and 10 C, respectively. LFP2/C delivers discharge capacities of 160 mA h g^{-1} (0.1 C), 139 mA h g^{-1} (1 C), 120 mA h g^{-1} (5 C), and 95 mA h g^{-1} (10 C). The samples exhibit comparable performances at low rates, but at higher rates the performance of the LFP1/C composite is superior. The capacity of LFP1/C exceeds that of LFP2/C by 12 and 15 mA h g^{-1} at 5 C and 10 C, respectively (Table 2). The rate performances of other $LiFePO_4$ nanowires synthesized by electrospinning are also listed in Table 2. The nanoscale LFP1/C particles showed a higher rate capability than those of $LiFePO_4$ nanowires. It is concluded that grain size and grain-size distribution are more important to electrochemical performance than morphology.

LFP1/C also has superior cycling properties, as shown in Fig. 7. It provides long-term cyclability, with a capacity loss of less than 3 % at 0.1 C and 5 % at 5 C after 500 cycles. The charge/discharge curves of the first, 100th, 200th, 300th, 400th, and 500th cycles at a rate of 5 C are displayed in the inset of Fig. 7. The discharge voltage plateaus of 3.35 V remains nearly the same as that of the first cycle, and the difference between the charge and corresponding discharge potentials remains constant. These results highlight the fact that the higher discharge capacities and better rate capabilities of LFP1/C are directly related to the nanosized particles and uniform nanoparticle distribution of the samples; these properties are attributed to the effective control of the nanofiber precursor using an electrospinning-assisted method.

Conclusions

Nano-$LiFePO_4$/C is prepared using a simple electrospinning method to control the particle size at the nanometer level, with PVP as a fiber-forming and carbon source. The PVP polymer matrix not only tailors the particle shape but also helps to maintain the connectivity between nanoparticles as a result of its residual conductive carbon after high-temperature pyrolysis, thereby impeding crystal growth and increasing the conductivity.

Compared with samples obtained using the normal ball-milling method, samples produced using the electrospinning method consist of nano-$LiFePO_4$ particles and have a better electrochemical performance. The nano-$LiFePO_4$/C cathode exhibited high capacities under different charge/discharge rates (from 0.1 C to 10 C) upon cycling from 2.5 to 4.2 V. The expanded rate capability of the electrode is accompanied by superior cycle stability, which can be ascribed to the synergistic effect of the highly conductive carbon network and nanoscale $LiFePO_4$/C particles.

Acknowledgments This work was supported by a project issued by the National Key Technologies R&D Program of China (grant no. 2009BAG19B00) and National High Technology Research and Development Program of China (863 Program, no. SS2012AA110301).

References

1. Padhi AK, Nanjundaswamy KS, Goodenough JB (1997) J Electrochem Soc 144:1188–1194
2. Nakamura T, Miwa Y, Tabuchi M, Yamada Y (2006) J Electrochem Soc 153:A1108–A1114
3. Ni JF, Zhou HH, Chen JT, Zhang XX (2005) Mater Lett 59:2361–2365
4. Wang D, Li H, Shi S, Huang X, Chen L (2005) Electrochim Acta 50:2955–2958
5. Chung SY, Bloking JT, Chiang YM (2002) Nat Mater 1:123–128
6. Park KS, Scougaard SB, Goodenough JB (2007) Adv Mater 19:848–851
7. Dominko R, Bele M, Goupil JM, Gaberscek M, Hanzel D, Arcon I, Jamnik J (2007) Chem Mater 19:2960–2969
8. Sun LQ, Li MJ, Cui RH, Xie HM, Wang RS (2010) J Phys Chem C 114:3297–3303
9. Yamada A, Chung SC, Hinokuma K (2001) J Electrochem Soc 148:A224–A229
10. Prosini PP, Carewska M, Scaccia S, Wisniewski P, Pasquali M (2003) Electrochim Acta 48:4205–4211
11. Kim HS, Cho BW, Cho WI (2004) J Power Sources 132:235–239
12. Hsu KF, Tsay SY, Hwang BJ (2004) J Mater Chem 14:2690–2695
13. Ni JF, Morishita M, Kawabe Y, Watada M, Takeichi N, Sakai T (2010) J Power Sources 1950:2877–2882
14. Yang MR, Ke WH, Wu SH (2005) J Power Sources 146:539–543
15. Sides CR, Croce F, Young VY, Martin CR, Scrosati B (2005) Electrochem Solid-State Lett 8:A484–A487
16. Liu J, Liu FK, Yang GL, Zhang XF, Wang JW, Wang RS (2010) Electrochim Acta 55:1067–1071
17. Muraliganth T, Murugan AV, Manthiram A (2008) J Mater Chem 18:5661–5668
18. Greiner A, Wendorff JH (2007) Angew Chem Int Ed 46:5670–5703
19. Thavasi V, Singh G, Ramakrishna S (2008) Energy Environ Sci 1:205–221
20. Ramaseshan R, Sundarrajan S, Jose R, Ramakrishna S (2007) J Appl Phys 102:111101–111117
21. Li D, Xia YN (2004) Adv Mater 16:1151–1170
22. Uyar T, Havelund R, Nur Y, Hacaloglu J, Besenbacher F, Kingshott P (2009) J Membr Sci 332:129–137
23. Hosono E, Wang Y, Kida N, Enomoto M, Kojima N, Okubo M, Matsuda H, Saito Y, Kudo T, Honma I, Zhou H (2009) Appl Mater Interfaces 2:212–218
24. Zhu CB, Yu Y, Gu L, Weichert K, Maier J (2011) Angew Chem Int Ed 50:6278–6282
25. Ramakrishna S (2005) An introduction to electrospinning and nanofibers. World Scientific, River Edge
26. Wang LN, Zhan XC, Zhang ZG, Zhang KL (2008) J Alloys Compd 456:461–465
27. Murugan AV, Muraliganth T, Manthiram A (2008) J Phys Chem C 112:14665–14671
28. Wu XL, Jiang LY, Cao FF, Guo YG, Wan LJ (2009) Adv Mater 21:2710–2714
29. Yan XD, Yang GL, Liu J, Ge YC, Xie HM, Pan XM, Wang RS (2009) Electrochim Acta 54:5770–5774